Design and Application of a New Automated Fluidic Visceral Stimulation Device for Human fMRI Studies of Interoception

Jarrahi, Behnaz ; Gassert, Roger ; Wanek, Johann ; Michels, Lars ; Mehnert, Ulrich ; Kollias, Spyros S

Abstract: Mapping the brain centers that mediate the sensory-perceptual processing of visceral afferent signals arising from the body (i.e., interoception) is useful both for characterizing normal brain activity and for understanding clinical disorders related to abnormal processing of visceral sensation. Here, we report a novel closed-system, electrohydrostatically driven master-slave device that was designed and constructed for delivering controlled fluidic stimulations of visceral organs and inner cavities of the human body within the confines of a 3T magnetic resonance imaging (MRI) scanner. The design concept and performance of the device in the MRI environment are described. In addition, the device was applied during a functional MRI (fMRI) investigation of visceral stimulation related to detrusor distention in two representative subjects to verify its feasibility in humans. System evaluation tests demonstrate that the device is MR-compatible with negligible impact on imaging quality [static signal-to-noise ratio (SNR) loss <2.5% and temporal SNR loss <3.5%], and has an accuracy of 99.68% for flow rate and 99.27% for volume delivery. A precise synchronization of the stimulus delivery with fMRI slice acquisition was achieved by programming the proposed device to detect the 5 V transistor-transistor logic (TTL) trigger signals generated by the MRI scanner. The fMRI data analysis using the general linear model analysis with the standard hemodynamic response function showed increased activations in the network of brain regions that included the insula, anterior and mid-cingulate and lateral prefrontal cortices, and thalamus in response to increased distension pressure on viscera. The translation from manually operated devices to an MR-compatible and MR-synchronized device under automatic control represents a useful innovation for clinical neuroimaging studies of human interoception.

DOI: https://doi.org/10.1109/JTEHM.2016.2538239

IEEE Journal of Translational Engineering in Health and Medicine

Received 17 October 2015; revised 7 January 2016; accepted 29 February 2016.
Date of publication 31 March 2016; date of current version 20 April 2016.

Digital Object Identifier 10.1109/JTEHM.2016.2538239

Design and Application of a New Automated Fluidic Visceral Stimulation Device for Human fMRI Studies of Interoception

BEHNAZ JARRAHI[1,2], (Member, IEEE), ROGER GASSERT[3], (Senior Member, IEEE), JOHANN WANEK[4], LARS MICHELS[1], ULRICH MEHNERT[4], AND SPYROS S. KOLLIAS[1]

[1]Clinic for Neuroradiology, University Hospital Zurich, Zürich 8091, Switzerland
[2]Department of Psychiatry and Biobehavioral Sciences, Semel Institute for Neuroscience and Human Behavior, University of California at Los Angeles, Los Angeles, CA 90095, USA
[3]Department of Health Sciences and Technology, Institute of Robotics and Intelligent Systems, ETH Zurich, Zürich 8092, Switzerland
[4]Spinal Cord Injury Center, Balgrist University Hospital, Zürich 8008, Switzerland

CORRESPONDING AUTHOR: B. JARRAHI (behnazj@ucla.edu)

This work was supported in part by the Swiss National Science Foundation under Grant 135774.

ABSTRACT Mapping the brain centers that mediate the sensory-perceptual processing of visceral afferent signals arising from the body (i.e., interoception) is useful both for characterizing normal brain activity and for understanding clinical disorders related to abnormal processing of visceral sensation. Here, we report a novel closed-system, electrohydrostatically driven master–slave device that was designed and constructed for delivering controlled fluidic stimulations of visceral organs and inner cavities of the human body within the confines of a 3T magnetic resonance imaging (MRI) scanner. The design concept and performance of the device in the MRI environment are described. In addition, the device was applied during a functional MRI (fMRI) investigation of visceral stimulation related to detrusor distention in two representative subjects to verify its feasibility in humans. System evaluation tests demonstrate that the device is MR-compatible with negligible impact on imaging quality [static signal-to-noise ratio (SNR) loss $<2.5\%$ and temporal SNR loss $<3.5\%$], and has an accuracy of 99.68% for flow rate and 99.27% for volume delivery. A precise synchronization of the stimulus delivery with fMRI slice acquisition was achieved by programming the proposed device to detect the 5 V transistor–transistor logic (TTL) trigger signals generated by the MRI scanner. The fMRI data analysis using the general linear model analysis with the standard hemodynamic response function showed increased activations in the network of brain regions that included the insula, anterior and mid-cingulate and lateral prefrontal cortices, and thalamus in response to increased distension pressure on viscera. The translation from manually operated devices to an MR-compatible and MR-synchronized device under automatic control represents a useful innovation for clinical neuroimaging studies of human interoception.

INDEX TERMS MR-compatible sensors and actuators, fMRI, electrohydrostatic actuation, automation, visceral afferent processing.

I. INTRODUCTION

The development of modern neuroimaging techniques, in particular, blood-oxygen-level-dependent (BOLD) functional magnetic resonance imaging (fMRI) made it possible to study the brain networks that subserve sensory processing and related perceptual phenomena. As the scientific understanding of the neural correlates of the exteroceptive sensory modalities such as vision, audition, olfaction, gustation (taste), and somatosensation (e.g., cutaneous mechano-reception and proprioception) is increasing over time, the mechanisms underlying cerebral modulations of the interoceptive systems [1] have remained underrepresented in the existing fMRI literature (except perhaps in the area of human nociception [2]). In recent years, however, there has been a renaissance of interest in studying the human interoceptive brain networks, in particular for the gastrointestinal and the urogenital systems, as the significance of the brain-viscera interactions in health

and their disruptions in various functional visceral diseases, such as gastroesophageal reflux, dyspepsia, irritable bowel syndrome, overactive bladder, and incontinence have become more evident [3]–[6].

Interoception is the ability to sense the psychophysiological condition of the body [1] such as the sensations that arise from the viscera and internal milieu including pain, organ pressure, and distention [7]–[9]. Neuroanatomical evidence suggests that the interoceptive-rich Aδ and C primary afferents enter the spinal cord through the lamina I of the dorsal horn of the spinal cord, and ascend in the contralateral lateral spinothalamic tract [10]. Since the major cortical targets of the thalamic projections from the lamina I neurons are the insula and the anterior cingulate cortex, these two brain regions are proposed to play an important role in processing visceral sensations [1], [11] with additional regions such as the prefrontal cortex are shown to become progressively involved as subjective awareness of feeling and volitional control of related actions emerges [12]–[15].

Visceral sensations that resemble real life situations are challenging to implement in MRI in part due to the difficulties involved in selectively stimulating a specific visceral organ in the MRI environment. The limited space within the magnet bore, and the posture of a subject lying on the scanner table (e.g., supine position) make it difficult to deliver visceral stimulations. The afferent signals often do not produce any obvious subjective experiences, consequently making it hard to rely on subjective assessment of interoceptive stimulation. Interoceptive awareness varies from diffused, vague feelings to distinctly sensed and localized perceptions that are projected to specific parts of the body schema [16]. Sensations from non-visceral sources can also mask visceral sensations by sensory gating and convergence mechanisms [17].

Despite these challenges, some promising work has been recently conducted to investigate interoceptive phenomena, such as the sensations that accompany digestion and elimination, in the confines of the magnet. In these fMRI studies, similar to the so-called interventional MRI techniques, a catheter or a tube was introduced into a body cavity or a visceral organ such as the esophagus, stomach and bladder, for administering various fluid substances to directly stimulate the chemo- or mechanoreceptors in the intended organ and elicit associated visceral sensations. Lassman et al. [18] inserted a fine-bore orogastric tube in participants' stomach and manually infused ingested lipid (dodecanoic acid) or sterile saline (control) into the stomach during fMRI for studying brain regions responding to ingested lipid and the role of the intestinal peptide cholecystokinin in mediating gut–brain signaling. Similarly, Van Oudenhove et al. [19] performed manual intragastric infusion of fatty acid solution or saline during fMRI while participants underwent neutral or sad emotion induction to investigate the interaction between nutrient-induced gut-brain signaling and sad emotion. To study regional brain activations in response to contact of esophageal mucosa with acid, Kern et al. [20] administered intraesophageal infusion of 0.1N HCl and compared the fMRI BOLD responses with those of saline infusion and balloon distention. To elucidate processing of urgency sensations, Mehnert et al. [21] catheterized subjects transurethrally and performed manual intravesical infusion of saline.

However, for an accurate interpretation of brain activity during visceral sensation in fMRI, it is essential to have complete control over the temporospatial properties of the visceral stimuli. Methodologically, manual administration of the fluid substances during a scan can be challenging especially because of an inadvertent variability of manual performance in task-related requirements such as timing, flow rate, and volumetric accuracy of infusion. This can be a major concern if different infusion volumes, flow rates or sequences of visceral infusion and drainage within an fMRI paradigm are envisioned, consequently requiring multiple manual adjustments of the flow rates during the course of a scan. Reoccurring breaks may not only create discomfort and distraction to a subject within the MRI scanner, but can also introduce artifacts and temporal inconsistencies in the acquired images. Due to the delayed time course of the BOLD fMRI signal compared to the neuronal activity [22], exact timing and precise stimulation intensity is necessary.

The aims of this study were (i) to design a new fluidic-based, MR-synchronized device that can deliver precise volumes of saline or biological fluids at a precise time to an internal organ inside a conventional 3T MRI scanner without interfering with imaging data acquisition, and (ii) to assess feasibility of using such a device during human fMRI. To implement fMRI studies using a mechatronic device, safety aspects and technical challenges must be overcome that are associated with introducing any new device to the fMRI environment [23]–[25]. A device is considered to be MR-compatible if it satisfies the following criteria: 1) it does not pose a health and safety hazard, 2) its introduction into the MRI environment does not affect the image quality, and 3) its operation remains unaltered when used inside the MRI environment [24], [25]. We addressed these challenges by designing a robust system, and subsequently tested its MR-compatibility and utility in a representative human fMRI experiment.

II. MATERIAL AND METHODS

A. SYSTEM ARCHITECTURE

A computer-controlled linear slide (Fig. 1a), comprising a bipolar stepper motor and a moving platform joined to a stationary base by a linear bearing system, is connected to a bi-directional pump that causes fluid flow and pressure changes in a hydraulic actuator. The pressurized hydraulic fluid transmits the energy through a closed-loop, flexible plastic pipeline to a slave cylinder inside the 3T MRI scanner room. In this closed-system configuration, positive or negative pressures in the slave cylinder result in a controllable movement of the slave piston, thus mirroring motions of the master cylinder outside the electromagnetic shield of the 3T MRI scanner room. A mechanical interface (Figs. 1b and 1c)

IEEE Journal of Translational Engineering in Health and Medicine

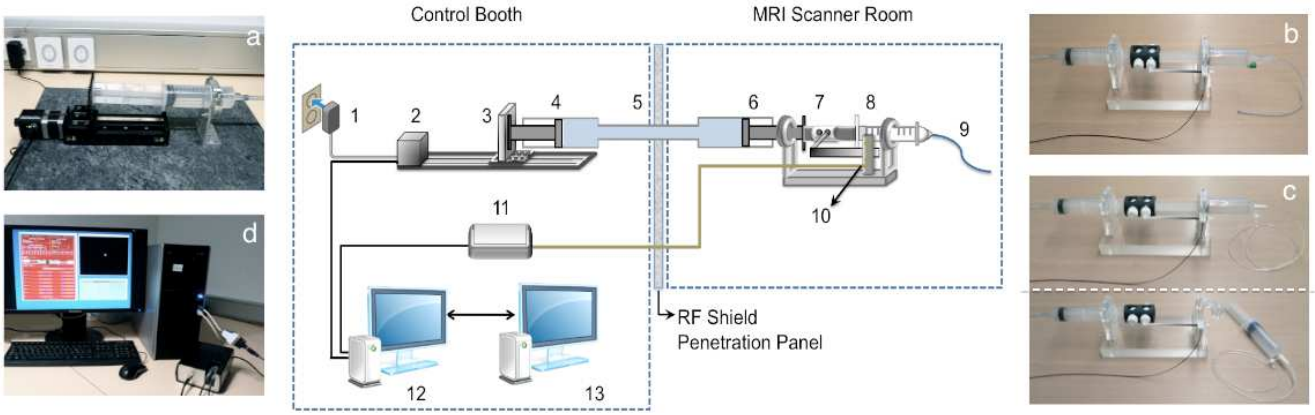

FIGURE 1. MR-compatible fluidic visceral stimulation device hardware. The device consists of: 1) AC power plug for stepper-motor-controlled linear slide, 2) motorized linear slide, which provides motion control via RS232 interface, 3) moving platform of the motorized linear slide and a right angle bracket that secures piston rod attachment to the moving platform, 4) master cylinder, 5) closed-loop 10 m flexible PVC tubing as a hydrostatic transmission line, 6) slave cylinder, 7) mechanical interface interconnecting coaxial slave piston to the syringe, 8) single-use syringe, 9) single-use catheter or tube, 10) MR-compatible fiber optic sensing unit, 11) fiber optic sensing unit's circuit board, 12) auxiliary PC where the operational control software runs, 13) MRI console PC; (a) Close-up view of the motorized linear slide and master cylinder rigidly attached to the moving plate of a linear slide by a 90-degree angle bracket; (b) The slave module containing the mechanical interface that interconnects the slave cylinder (left) to the infusion unit (right) including a 100 mL disposable syringe and a silicon catheter. The fiber optic sensing unit attaches to the mechanical interface that is placed inside the MRI scanner room as part of the slave module (the black cable in the picture is the 10-m fiber optic cable); (c) Another view of the slave module with an orogastric tube attached to a disposable 100 mL syringe. The disposable syringe and tube can be easily assembled (top) and disassembled (bottom) from the mechanical interface of slave module; (d) The auxiliary PC displaying the operational GUI. The box next to the PC is circuit board for the fiber optic sensing unit.

allows coupling of the slave piston and a syringe so that upon actuation of the device, the plunger in the syringe barrel is inserted or withdrawn in accordance with the motion of the slave piston, thus creating a dispensing or aspirating effect to infuse or drain fluid from the subject's visceral organ or internal body cavity through a connected catheter or tube. Most notably, the closed-system configuration means that the hydraulic fluid that is contained inside the master-slave system is separated from the fluid (e.g., saline or biological fluids) that is directly infused into or drained out of the subject's body.

The key components of the closed-system device (Fig. 1, center) include a pair of double-action hydraulic master and slave pistons, each encased in a plastic chamber made from modified 140 mL polyethylene/polypropylene Monoject piston syringes (Covidien-Kendall, USA), 10 m flexible PVC tubing with an inside diameter of 6 mm and wall thickness of 1.5 mm (Emil Lux GmbH & Co., Germany), a custom-made MR-compatible fiber optic sensor unit (detailed below), a motorized linear slide (model T-LSR 150B) with 150 mm travel and 0.5 μm resolution (Zaber Technologies Inc., Canada), a 90 degree angle bracket (AB90-M, Zaber Technologies Inc., Canada), which rigidly secures the master piston rod to the moving plate of the slider, and an infusion unit. The infusion unit includes a sterile single-use 100 mL medical-grade polyethylene/polypropylene syringe (Omnifix, B Braun Melsungen AG, Germany) that can be attached to a single-use polyurethane naso/orogastric feeding tube (CH/FR 15, Freka®Tube, Fresenius Kabi Ltd, UK) or a sterile single-use silicone catheter (CH/FR 14, UROMED Kurt Drews GmbH, Germany). The mechanical interface that interconnects two coaxial pistons by their plunger shafts was machined from plexiglass and polyacetal copolymer (Angst+Pfister, Switzerland).

TABLE 1. Specifications of the Fiber Optic Sensor

Parameter type	*Specification*
Sensing distance	25 mm
Light source	Pulsed red LED
Wave length	680 nm
Voltage supply range	10.8 to 26.4 VDC
Offset	0.75 to 1.5 V
Response time	1 to 50 ms (adjustable)
Analog voltage output	1.0 to 5.0 VDC
Load resistance	> 10 kΩ
Operating temperature	-20 to +60 ◦C
Adjustable resolution	0.3 to 6% (full scale)
Fiber-optic diameter	4.4 mm
Sensor probe head size	φ 6×24 (L) mm

The MR-compatible fiber optic sensing unit (indicated by an arrow and the label 10 in Fig. 1, center) comprises a reflective-type intensity modulated fiber optic sensor with an analogue voltage-output photodiode (FWDK 10U84Y0, Baumer Electric, Switzerland), a 10 m plastic sheathed, flexible fiber optic cable with two optical fibers as transceivers (FUE 999C1004, Baumer Electric, Switzerland), and a high-quality glossy photo paper on which a continuous gray spectrum is printed and attached to a thin polyacetal copolymer rod with 1 cm in diameter. The technical specifications of the fiber optic sensor are summarized in Table 1. The sensor

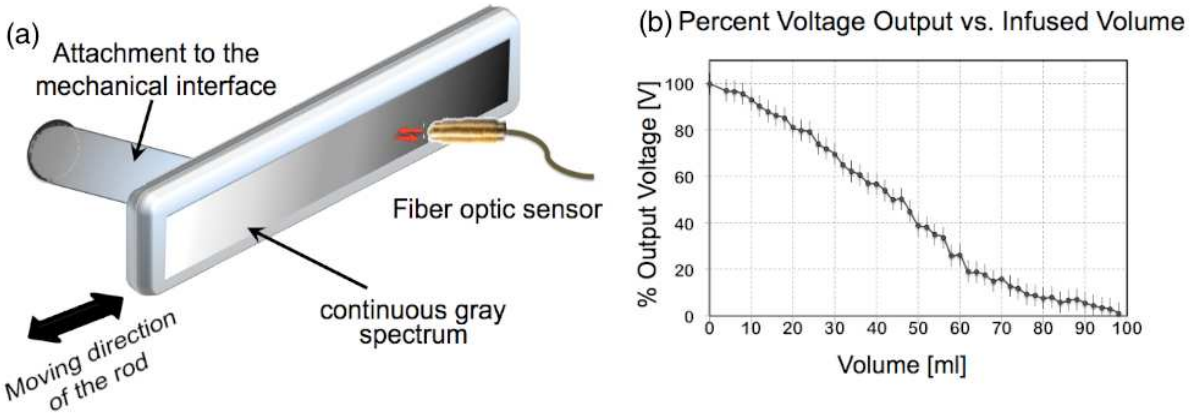

FIGURE 2. **MR-compatible fiber optic sensing unit for the slave module (a) Sensing principle; (b) Relationship between the percent output voltage generated by the fiber optic sensor and the discharged volume from the 100 mL syringe in the slave module. Error bars indicate standard errors of the mean of three measurements.**

is attached to the mechanical interface placed inside the 3T MRI scanner room using a rubber gasket and brass screws. The sensing principle of this unit is illustrated in Fig. 2a. As the mechanical interface moves, the rod holding the gray spectrum moves accordingly in front of the stationary fiber optic sensor. Changes in the optical reflection properties produce differential output signals from the sensor (Fig. 2b), and quantification of parameters including relative linear displacement and velocity of the slave module are calculated from optical sensor's output voltage. We used a 15V AC-to-DC converter (PM10-15, Mean Well Inc., USA) to provide required power for the optical sensor, and included a 12-bit multifunction USB data acquisition card (DAQ USB-6008, National Instruments) to sample signals from the sensor during the operation of the device (Fig. 3). The interface card also detects the 5 V transistor-transistor logic (TTL) trigger signals generated by MRI scanner at each radiofrequency excitation pulse to synchronize the device movements with image acquisition during fMRI.

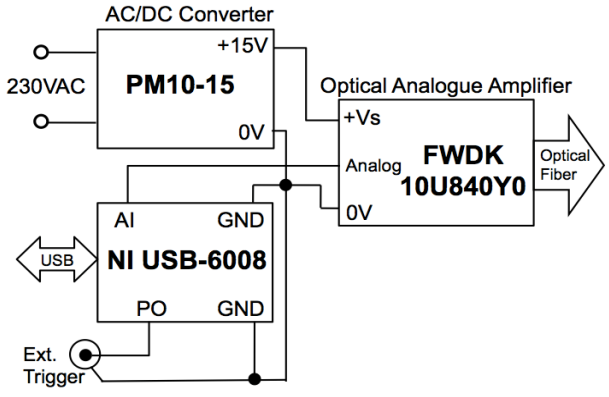

FIGURE 3. **Slave module optical sensing unit circuit board. The board includes a power supply, a data acquisition card, and an optical amplifier placed outside the MRI scanner room in the control booth to prevent image artifacts and other issues related to the non-MR-compatibility of the circuit board components.**

The safety criterion requires that the interactions between a device and MRI scanner should not cause health and safety hazards [23]–[25]. Primary interactions between a device and the MRI scanner include the magnetically induced forces and torques, radiofrequency-induced heating, and induction of voltages [26]. For optimum safety and MR-compatibility, these interactions must be properly controlled [27]. In addition, the device should guarantee that the fluid, which is infused into or drained out of a subject's visceral organ or body cavity, does not leak or become contaminated during its operation, because if this happens, it can expose the subject to serious biohazards, increase the risk of residual cross-contamination between successive subjects, and possibly hinder the function of the device. The problem of residual cross-contamination between subjects is a serious concern due to the many known diseases that can be communicated by the transfer of infected body fluids between subjects especially in clinical settings. Therefore, any section of the device coming into direct contact with the subject's internal cavity should be sterile, and securely mountable to the system to prevent any possible contamination or leakage of fluid. The use of a disposable, single-use catheter or tube with a single-use plastic syringe in the infusion unit of the device (the only section of the device that comes into a direct contact with a subject's body) guarantees sterile conditions and good clinical practice during operation. Additionally, distilled water was used as working fluid inside the closed-system instead of conventional petroleum or mineral oil to maintain a clean, non-polluting system inside the MRI environment.

The control of the flow rate is accomplished by the control of the position and speed of the stepper-motor-controlled linear slide through feedback signals from the slave module fiber optic sensing unit. A block diagram representation of the operational control software developed for this device is shown in Fig. 4. We leveraged the build-in motion controller provided by Zaber Technologies, and programmed a central operational controller interface in C++ using Visual Studio 2010 (Microsoft, USA) running under the Windows

IEEE Journal of Translational Engineering in Health and Medicine

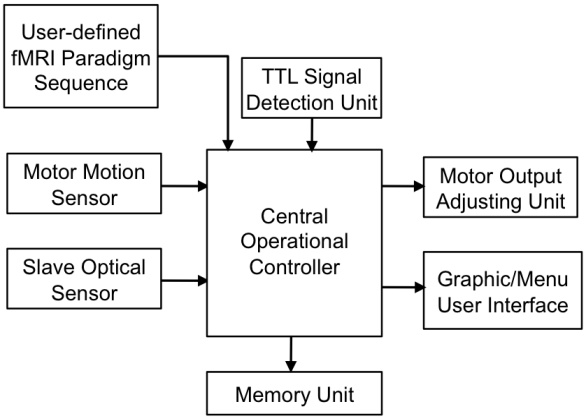

FIGURE 4. Block diagram representation of the MR-compatible fluidic visceral stimulation device operational control software. The custom-designed software includes an input unit that receives a user-defined fMRI paradigm sequence, a TTL signal detection unit for starting the operation and synchronizing the system function with the acquisition of functional volumes by the MRI scanner, a motor motion sensor for sensing the actual motor speed and traveling distance, an optical sensing unit for measuring the traveling distance and velocity of the slave module, a memory unit for storing the system variables as logs, and a GUI for displaying the system status to a user during fMRI.

operating system with a graphical user interface (GUI) for user input. The custom-made software allows users to define system parameters such as flow rate, and delivery volume. The GUI consists of an easy-to-use menu for various actions such as: choosing a specific fMRI paradigm, synchronizing the stimulation process with the acquisition of functional volumes through detection of the TTL pulses from the MRI scanner, controlling the stepper-motor-controlled linear slide, monitoring displacement of slave pieces for output flow rate accuracy, connecting to external devices such as a response box, and storing the operation variables as a log file for future reference.

B. DEVICE TESTING PROCEDURE

We performed a series of MR-compatibility tests, and evaluated the system performance in terms of flow rate and volume delivery accuracy at the MRI center of the University Hospital Zurich on a 3T whole-body MRI scanner (Ingenia, Philips Medical Systems) with a standard 15-channel head coil array. For MR-compatibility tests, the imaging object was a 3,000 mL cylindrical liquid phantom (Philips P/N 452213081924, diameter: 13.5 cm, height: 30 cm) containing 1,000 mL of demineralized water with 770 mg $CuSO_4$ $5H_2O$, 2,000 mg NaCl, 1 mL arquad (1% solution), and 0.15 mL H_2SO_4 (0.1 M solution). Functional images sensitive to BOLD contrast were acquired in an ascending fashion with 34 axial slices (each 3.0 mm thick, 1.0 mm inter-slice gap) using a T2*-weighted, single-shot, field echo, echo-planar imaging (EPI) sequence (TE/TR = 30/2000 ms, flip angle = 80°, field of view = 240 mm × 240 mm, image matrix = 96 × 96). The following conditions were tested on a phantom while an MR volume of thirty-one dynamic slices were acquired for each condition: (a) without the presence of the system (more specifically the slave module) in the MRI scanner room (i.e., phantom only; ''Baseline''), (b) with the slave module installed in the 3T MRI scanner room but powered off (''Installed''), (c) with the installed slave module in the 3T MRI scanner room with the active components powered on but not actuated (''Powered''), and (d) with the installed slave module in the 3T MRI scanner room with the active components powered on and actuated (''Actuated''). When present, the installed slave module was placed next to the 3T MRI scanner bore on the scanner table about 40 cm away from the base of the phantom. This distance is the typical working distance for visceral stimulation of the gastrointestinal tract (e.g., stomach, esophagus) but closer than the typical working distance of 50–60 cm for stimulating the urogenital system (e.g., bladder). We chose the 40-cm distance to emphasize the effects of the slave module's presence near the phantom. The phantom was placed in the head coil and was kept immobilized with foam pads during the scan. In each test iteration, in addition to the EPI imaging protocol, we also acquired anatomical images (3D T1-FFE [Fast Field Echo], 3.1 ms TE, 6.9 ms TR, 8° flip angle, 256 mm × 256 mm field of view, 256 × 256 matrix, voxel size = 1 mm × 1 mm × 1 mm, 180 slices), and magnetic field map (3D T1-FFE, 2.3 ms TE1, 4.6 ms TE2, 20 ms TR, 10° flip angle, 240 mm × 240 mm field of view, 80 × 80 matrix, 3.0 mm thickness, 50 slices) for added image quality analysis. The ambient room air temperature was held constant at around 25°C during the entire test period.

Both quantitative and qualitative methods were used to evaluate the MR-compatibility of the fluidic visceral stimulation device. For qualitative assessments, we evaluated the static signal-to-noise ratio (SNR), the time variant (temporal) signal-to-noise ratio (tSNR) and image homogeneity (uniformity) as a measure of spatial image quality, image time course stability, and spatial homogeneity of the MR image, respectively. The static SNR values for each condition were calculated for anatomical and functional images according to the signal-background method by dividing the mean signal intensity over the standard deviation of background signal noise corrected with the Rayleigh distribution factor [28]. For an acquired MR image, the signal intensity was calculated by taking the mean voxel intensity value in a homogenous circular region of interest (ROI) within the phantom, while the noise was computed from the background air voxel by defining four smaller ROIs outside the phantom (free of phase-encode ghosting artifacts). The tSNR for each condition was calculated voxelwise only for functional images as the ratio between the mean signal intensity of the time series x_i and its temporal standard deviation as in (1):

$$tSNR = \frac{\mu}{\sqrt{1/N \sum_{i=1}^{N} (x_i - \mu)^2}} \tag{1}$$

where N is the number of time points [29]. Although the static SNR is typically used to compare imaging hardware

or acquisition methods [30], the tSNR may be a better proxy for fMRI performance because the static SNR reflects only static noise or single MR image signal strength over the noise present in the absence of signal [29]. The functional image homogeneity was calculated using (2) as proposed by the American Association of Physicists in Medicine (AAPM) protocol [31]:

$$Homogeneity = 100\% \times \left(1 - \frac{Max - Min}{Max + Min}\right) \qquad (2)$$

where Max and Min are the maximum and minimum image signal intensities of the ROI inside the imaging phantom. To check whether the static SNR and tSNR were significantly changed in any condition, one-sample t-test was performed using R statistical software (version 3.1.0, http://www.r-project.org) where $p < 0.05$ was considered to be statistically significant.

For the qualitative evaluation, in addition to visually inspecting all MR images (anatomical, functional, and field maps) for the presence of an artifact, we performed image quality checks by image subtraction method in the following manner: the binary image data of acquisitions from each condition were subtracted pixel by pixel from the baseline condition (i.e., phantom only, no device), resulting in difference images. The slice positioning was the same, and every EPI slice was analyzed separately for each condition. Image analysis was performed using an in-house-written MATLAB script. Furthermore, the magnetically induced displacement force was measured indirectly via a deflection angle between the magnetically induced force of a device and its force due to gravity as described in [32].

To evaluate the performance quality of the device, we measured the flow rate and volume delivery accuracy outside the 3T MRI scanner room with a Cubemass DCI Coriolis flow meter (Endress + Hauser, Switzerland, instrument errors of 0.1%). Five flow rates from 100 to 500 mL/min in 100 mL/min increments were used to test the system performance. For each flow rate, we performed three repetitive infusion and drainage cycles of 100 mL of sterile solution of 0.9% NaCl (B Braun Melsungen AG, Germany) at room temperature (~25°C). Next, we repeated the same experiment inside the 3T MRI scanner room during functional imaging scanning and also while the scanner was quiescent. To evaluate the performance of the device in the MRI environment, a custom-designed apparatus was used to record the infusion and drainage rates and transferred volumes (Fig. 5). A silicone catheter with a conical Nelaton tip (CH/FR 14, UROMED Kurt Drews GmbH, Germany) was first attached to a 100 mL polyethylene/polypropylene syringe (Omnifix, B Braun Melsungen AG, Germany) filled with 100 mL sterile solution of 0.9% NaCl (B Braun Melsungen AG, Germany) at room temperature. The syringe was attached to the slave cylinder through the mechanical interface. The slave module was placed on the MRI scanner table about 40 cm away from the phantom base. The distal end of the catheter was inserted into an empty 120 mL transparent plastic

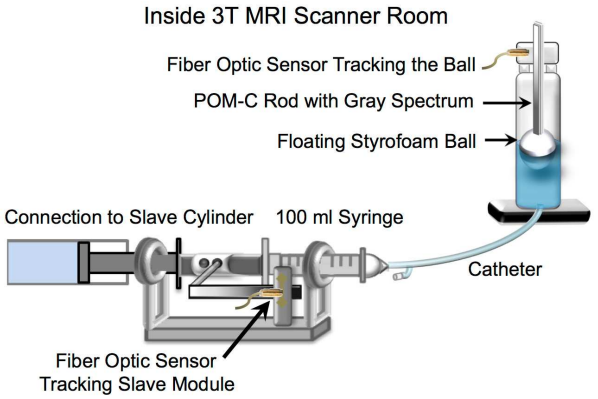

FIGURE 5. Experimental setup for evaluating the system performance inside 3 Tesla MRI scanner. A silicone catheter was attached to a 100 mL syringe connected to the slave cylinder through the mechanical interface and placed on the scanner table about 40 cm away from the base of the phantom. The distal end of the catheter was inserted inside an empty PET container, where an optical sensor was carefully positioned on top of it. A floating styrofoam ball with a thin plastic rod holding a printed gray spectrum line was placed inside. As the container filled, the styrofoam ball remained on the water surface while the spectrum moved upward resulting in change in voltage output from the optical sensor, which was recorded and saved on a computer during the testing.

(polyethylene terephthalate; PET) container, and the dispensed saline was collected in this container. A similar optical sensor to the one that was used in the slave displacement sensor, but with a slightly larger sensing range (FUE 500C1003, Baumer Electric, Switzerland) was carefully positioned at the top of the plastic collecting bottle as shown in Fig. 5. A floating styrofoam ball was placed at the bottom of the empty plastic container with a thin polyacetal copolymer rod inserted into the center of the ball. A high-quality glossy photo paper with a printed continuous spectrum of gray was glued to the rod and placed facing the fiber optic sensor. As the container filled, the styrofoam ball remained on the water surface while the rod moved upward resulting in change in the voltage output from the optical sensor. Data from both optical sensors (i.e., optical displacement sensor and optical sensor tracking the ball) were logged onto a desktop computer and processed using a custom-developed software program (LabVIEW, National Instruments). During the test, the volume of the infusate and the linear displacement of the slave module were recorded continuously as a function of the respective optical sensor signal output and saved on the computer. At the end of each test, the infusion rate was calculated by converting the output voltage to discharged volume and subtracting the volume at a given time (V_t) from that obtained at the next time point ($V_{[t+\Delta t]}$) as in (3):

$$Q = \frac{V_t - V_{(t+\Delta t)}}{\Delta t} \qquad (3)$$

where t is the time in seconds. The values were multiplied by 60 to obtain flow rates in ml/min. Data were reported as mean ±SD. The accuracy of each parameter was calculated as the difference between the set value and measured mean value in percent, while the precision was computed as the standard

IEEE Journal of Translational Engineering in Health and Medicine

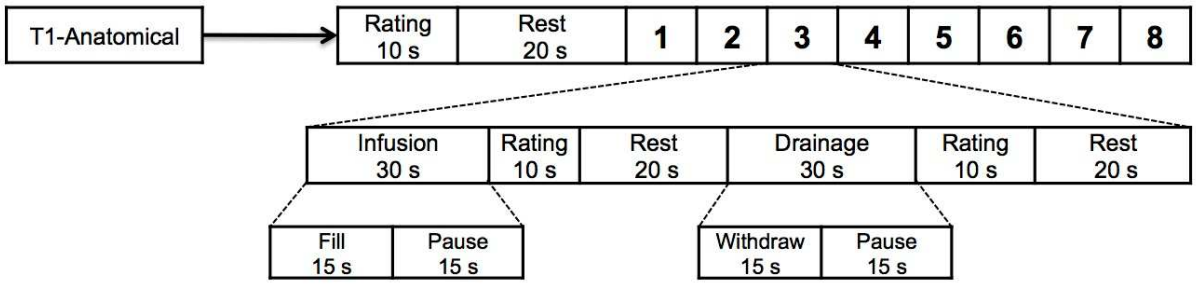

FIGURE 6. Scanning protocol and fMRI task sequence. The fMRI measurements started with initial 10-second subject rating followed by 20-second rest. Subsequently 90 mL room temperature saline was repeatedly infused and drained intravesically by the MR-compatible fluidic visceral stimulation device at the rate of 300 mL/min during fMRI. Eight blocks were performed with each block consisting of intravesical infusion (90 mL saline in 15 s then pause 15 s for a total time of 30 s), subject rating after intravesical infusion (10 s); rest (20 s), intravesical drainage (90 mL in 15 s then pause 15 s for a total time of 30 s), subject rating after intravesical drainage (10 s), and rest (20 s).

deviation of these differences. The performance of the system was also tested with an orogastric feeding tube (Freka®Tube, CH/FR 15, Fresenius Kabi Ltd, Warrington, UK) following the same experimental procedures and set up described above but only for infusion given that feeding tubes are generally used for visceral infusion in MRI.

C. HUMAN fMRI EXPERIMENT

Two right-handed [33] healthy subjects (both females, ages 21 and 47 years), with no history of neurological disorders, and no symptoms suggestive of urological dysfunction participated in return for payment. All subjects provided written informed consent to participate according to a protocol approved by the ethics committee of the canton of Zurich and in complete accordance with the Helsinki Declaration (http://www.wma.net/en/30publications/10policies/b3).

The visceral stimulation consisted of infusing then draining the bladder as a representative internal organ in a block design paradigm (Fig. 6) with 90 mL room-temperature sterile solution of 0.9% NaCl (B Braun Melsungen AG, Germany) at a rate of 300 mL/min followed by a pause to ensure adequate time for the slow visceral sensation to be registered before participants rated their desire to void sensation (sensation of fullness) on a 11-point scale with 0 being no desire to void and 10 having the strong desire to void. Subjects rated the intensity of their feelings by the use of a custom-built MR-compatible handheld optical response system that we developed before [34], [35]. The response box was held in the dominant right hand and included an analog input device (i.e., a scrolling wheel or knob), which was set to traverse the entire rating range with minimal thumb/index finger twisting. The visual feedback consisted of a 11-point visual analog scale (VAS) that was projected via an LCD projector onto a translucent screen that stood at the foot of the gantry of the MRI scanner. The subjects viewed the screen from inside the scanner through a mounted mirror attached to the head coil positioned above their eyes at a 45° angle. Prior to the fMRI scan, subjects were catheterized transurethrally with a silicone catheter (CH/FR 14, UROMED Kurt Drews GmbH, Germany). After the initial intravesical filling with 100 mL saline, the catheter was attached to the fluidic visceral stimulation device and the fMRI scan begun with initial subject rating (10 seconds) followed by a 20-second initial rest before automated intravesical filling and subsequent saline withdrawal was initiated using the MR-compatible fluidic visceral stimulation device. A precise synchronization of the stimulus delivery with fMRI slice acquisition was achieved by the detection of the 5V TTL trigger signals generated by the 3T MRI scanner at each radiofrequency excitation pulse. The imaging data were acquired on the same MRI scanner (3T Ingenia, Philips Medical Systems) using the same scanning parameters that we used for MR-compatibility tests.

Imaging data were preprocessed using Statistical Parametric Mapping software (SPM12; Wellcome Department of Cognitive Neurology, UK). The functional images were realigned to correct for head movements, co-registered to the T1 anatomical images, and normalized into the Montreal Neurological Institute (MNI) stereotaxic coordinates system using the EPI template provided with SPM12, and smoothed with a Gaussian profile filter of full-width-half maximum of 8 mm. The fMRI data were analyzed using a general linear model (GLM) approach with the standard hemodynamic response function [36]. Signal intensity time course for each voxel was linearly determined to model two task design-related regressors (i.e., intravesical saline infusion, and intravesical saline drainage) and two regressors of no-interest (i.e., subject ratings after intravesical infusion, and subject ratings after intravesical drainage) by convolving corresponding fMRI time-series with the canonical hemodynamic response function. For the main effect, statistical parametric maps of the t-statistic (SPM[t]) reflecting the BOLD signal change were calculated for the visceral stimulation (i.e., intravesical saline infusion) versus rest ($p < 0.05$ corrected for multiple comparisons using the family-wise error (FWE), correction for the whole brain). Activation maps were overlaid on a high-resolution structural image in the MNI orientation (supplied with SPM12 software package).

TABLE 2. Image Quality Metrics for the Device MR-Compatibility Tests With a Phantom.

Test Condition	Anatomical SNR	Functional SNR	Functional tSNR	% Image Homogeneity
Baseline	75.99 ± 2.32	70.512 ± 1.36	73.807 ± 2.15	100
Installed	75.62 ± 1.91 (0.427)	70.501 ± 1.34 (0.491)	73.796 ± 2.13 (0.490)	99.97
Powered	75.51 ± 1.76 (0.228)	70.501 ± 1.32 (0.492)	73.791 ± 2.04 (0.500)	99.87
Actuated	75.27 ± 0.11 (0.264)	70.497 ± 1.37 (0.489)	73.780 ± 2.12 (0.500)	99.55

* The *p*-value between a test condition and a baseline is shown in parentheses.

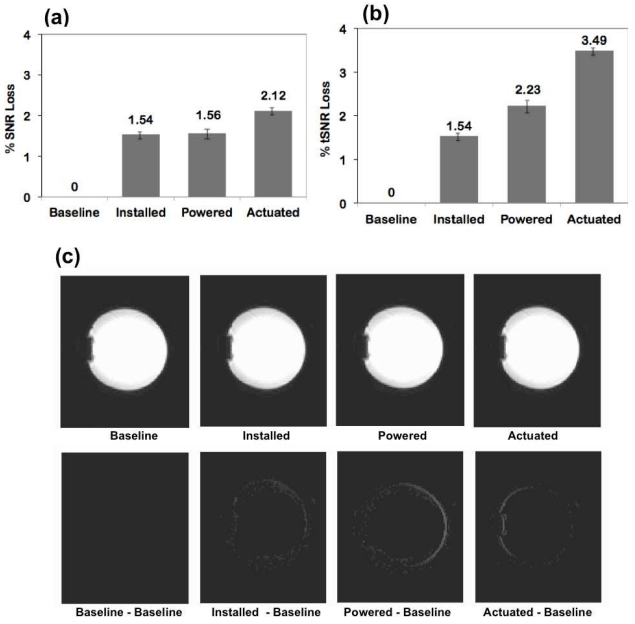

FIGURE 7. Quantitative and qualitative assessments of the device MR-compatibility. (a) Percent static SNR loss, and (b) Percent tSNR loss for functional images acquired under four different experimental conditions: without the presence of the device's slave module in the MRI scanner room ("Baseline"), with the slave module installed in the MRI scanner room but powered off ("Installed"), with the installed and powered on slave module ("Powered"), and with the installed, powered on, and actuated slave module ("Actuated"); (c) (Top) a graphical representation of phantom image for each testing condition. Middle slice (slice number 17/34) is shown here; (Bottom) image subtraction results.

TABLE 3. Flow Rate Measurements Inside 3T MRI Scanner Room

Set Flow Rate / *Condition*		100 mL/min	200 mL/min	300 mL/min	400 mL/min	500 mL/min
		Measured Flow Rate				
Scanner Running	Infusion	100.35 ± 0.56 mL/min	200.48 ± 3.08 mL/min	300.04 ± 3.77 mL/min	399.98 ± 1.95 mL/min	499.97 ± 3.96 mL/min
	Drainage	100.83 ± 1.78 mL/min	200.64 ± 2.94 mL/min	301.63 ± 1.87 mL/min	400.90 ± 4.59 mL/min	501.27 ± 5.69 mL/min
Quiescent Scanner	Infusion	100.66 ± 0.55 mL/min	201.87 ± 2.16 mL/min	300.93 ± 3.23 mL/min	400.36 ± 3.27 mL/min	499.91 ± 2.42 mL/min
	Drainage	99.11 ± 2.82 mL/min	201.54 ± 2.79 mL/min	300.61 ± 2.01 mL/min	399.32 ± 2.16 mL/min	501.88 ± 1.13 mL/min

III. RESULTS

A. DEVICE MR-COMPATIBILITY

The image quality metrics from different phantom test conditions and imaging modalities are summarized in Table 2. For none of the phantom condition, either the introduction of the slave module into the MRI environment or its powering and actuation caused any noticeable systematic impact on spatial or temporal image quality and homogeneity. During fMRI, the overall SNR and tSNR values over all slices in the MR phantom images decreased by no more than 3.5% across all testing conditions (Figs. 7a and 7b). The maximum degradation of the field homogeneity was less than 0.5%. The small differences between conditions were within normal expected variability range [37], and no statistical significant reductions in SNR or tSNR were observed ($p > 0.05$). The results of the qualitative functional image analysis by

TABLE 4. Volume delivery measurements inside 3T MRI scanner room.

Flow Rate / *Condition*		100 mL/min	200 mL/min	300 mL/min	400 mL/min	500 mL/min
		Volume of the delivered fluid (mL)				
Scanner Running	Infusion	101.33 ± 1.82 mL	100.57 ± 0.75 mL	100.57 ± 0.65 mL	100.32 ± 0.08 mL	100.73 ± 1.25 mL
	Drainage	100.05 ± 0.31 mL	100.25 ± 0.23 mL	100.29 ± 0.17 mL	99.54 ± 2.14 mL	100.31 ± 1.29 mL
Quiescent Scanner	Infusion	99.72± 0.24 mL	100.00 ± 0.10 mL	100.01± 0.34 mL	100.93 ± 2.11 mL	99.86 ± 0.73 mL
	Drainage	100.14 ± 0.24 mL	100.28 ± 0.81 mL	99.81 ± 0.69 mL	100.56 ± 0.41 mL	100.28 ± 0.67 mL

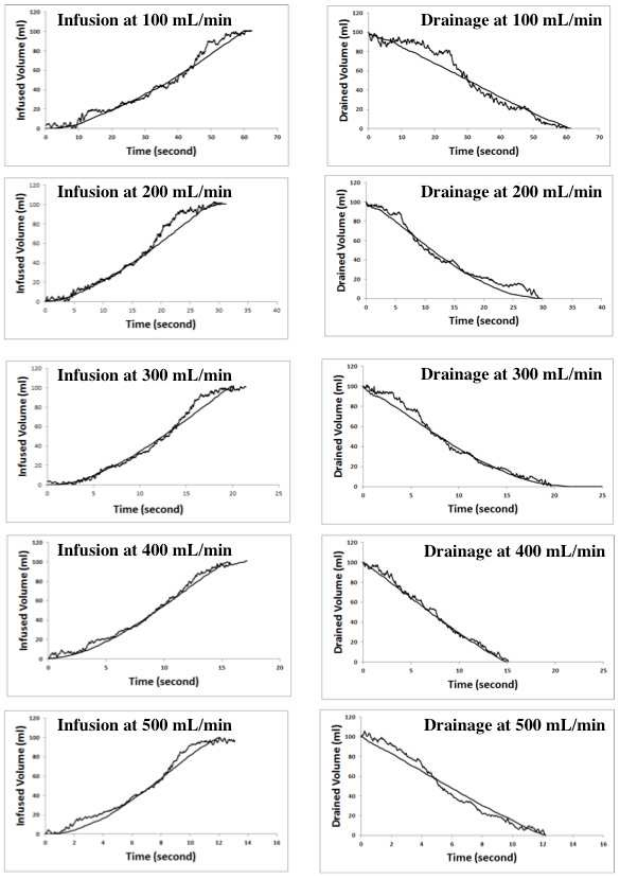

FIGURE 8. Sample infusion and drainage profiles obtained inside the 3T MRI scanner room while the scanner was running. Five different system flow rates (i.e., 100 mL/min, 200 mL/min, 300 mL/min, 400 mL/min, and 500 mL/min) were tested. In each plot, the smoother line corresponds to signal outputs of the slave module optical sensor while the other was recorded from the optical sensor tracking the floating styrofoam ball.

IEEE Journal of Translational Engineering in Health and Medicine

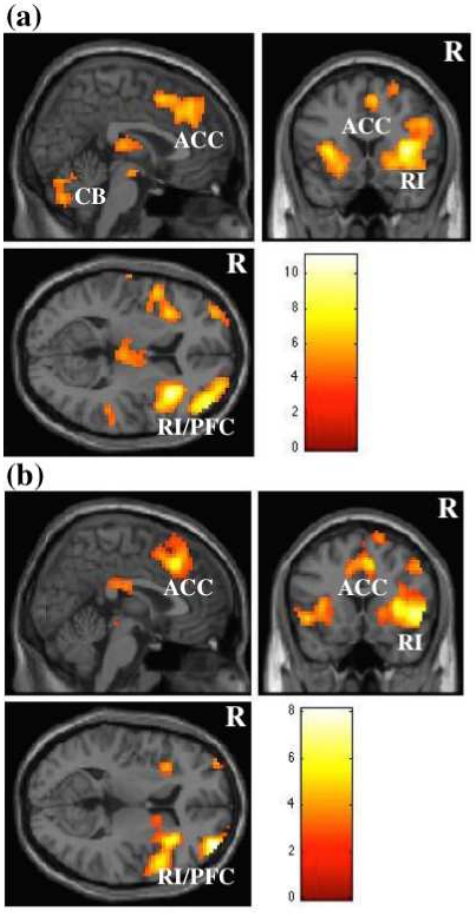

FIGURE 9. **Brain areas activated by intravesical infusion produced by the MR-compatible fluidic visceral stimulation device in two representative subjects. (a) Subject 1 (right-handed healthy female, 47 years) (b) Subject 2 (right-handed healthy female, 21 years); RI = right insula; ACC = anterior cingulate cortex; RI/PFC = right anterior insula and/or lateral prefrontal cortex; CB = cerebellum; R = right side. MNI coordinates: x = 3; y = 18; z = 10. Color bar shows scale of Student's *t*-values.**

image substation method are displayed in Fig. 7c. To relate the results to the expected BOLD signal changes in the fMRI experiments, the maximum deviation of the signal intensity in the center of the phantom was determined and results from the middle slice (slice number 17/34) are shown in Fig. 7c. The slices from other sections of the phantom had similar image quality in every condition. Visual inspection of all images including the field maps, showed no noticeable field deformations or radiofrequency interference associated with the presence of an external device in the vicinity of the 3T MRI scanner. Considering that the slave module (which is the only part of the device that is placed in the MRI scanner room) where made entirely form the durable polymeric materials devoid of any metallic pieces, there was no magnetic forces (i.e., no deflection angle) or device heating were observed during phantom MRI.

B. DEVICE PERFORMANCE

There was no difference in system performance with a catheter and with a tube present ($p > 0.05$). For clarity and due to lack of space, we only report results of system performance with a catheter. No differences in flow rate and volume delivery were found among different flow rates ($p > 0.05$); however, the accuracy and precision of flow rate and delivered volumes were slightly higher for slower flow rates. The average accuracy and precision for system flow rate, and delivered volumes over all tested flow rates were 99.68% and 99.27%, respectively. The measurements for the infusion and drainage flow rates and volume delivery performed inside the MRI scanner room are listed in Tables 3 and 4, respectively. There was no statistically significant difference between the measurements obtained with the quiescent scanner and with the scanner running ($p > 0.05$). Sample infusion and drainage profiles for different test flow rates while the scanner was running are shown in Fig. 8.

C. BOLD fMRI RESULTS

Imaging data from two healthy subjects were evaluated. For each subject, a general linear model was applied to the time course of the signal of each voxel. Individual statistical parametric maps for intravesical stimulation > rest contrast were calculated ($p < 0.05$, FWE-corrected for multiple comparisons). Whole brain activation maps from these two representative subjects are shown in Fig. 9. Consistent with previous publications [12], [21], standard GLM analysis revealed activation in the bilateral insula, the anterior and mid-cingulate cortex, the lateral prefrontal cortex, and the thalamus. For both subjects, insular activation is greater on the right. One of the subjects (subject 1) also showed activations in the brainstem and cerebellar areas. The mean $\pm$ SD of desire to void subject rating values after intravesical infusion, and after intravesical drainage were 2.01 ± 0.81, and 1.17 ± 1.02, respectively. None of the subjects reported any pain during the experiment.

IV. DISCUSSION AND CONCLUSION

A significant challenge in designing a device in direct contact with the viscera of the human body is its control principle and safety of operation. Using such a system in an MRI setting adds to the challenge level and necessitates careful thinking to select the appropriate principle of actuation. In this paper, we presented a novel closed-system, electrohydrostatically driven, optical feedback-controlled fluidic visceral stimulation device that can be safely used for BOLD fMRI studies investigating interoception of visceral organs. It permits passive non-painful stimulation relevant for research and clinical assessments of visceral organs in the confines of the 3T magnet. All sections of the device that are placed inside the MRI scanner room are entirely made of durable polymeric materials, and no ferromagnetic parts are present to interfere with image quality. Due to the merit of the electrohydrostatic actuation in separating the two actuated platforms through a hydrostatic transmission line, the device is proved to be MR-compatible with negligible impact on MRI data quality (static SNR loss < 2.5%,

and tSNR loss $< 3.5\%$). To achieve consistent system performance in relation to delivered fluid flow rate and volume, and for logistical safety reasons, we also implemented a fiber optic sensing unit for the slave module and freely-programmable (C++) hardware components. The custom software synchronizes the system with the MRI scanner by detecting the TTL trigger signals generated by the MRI scanner, receives feedback signals from the fiber optic sensing unit, and continuously monitors the critical system parameters during fMRI. Accordingly, this device showed excellent performance quality (flow rate and volume delivery accuracy $> 99\%$).

The utility of this device to deliver visceral stimulation to internal organs in supine position during an actual fMRI experiment was tested in two healthy volunteers. By delivering the fluid directly into a visceral organ (here, the bladder was used as an example) at a pre-defined intensity (i.e., flow rate and volume), which was not perceptible to subjects (as shown by persistent low urgency sensation even after intravesical infusion of 90 mL saline), we were able to identify precisely those temporospatial responses attributable to brain-viscera signaling pathway. By contrasting BOLD signals during the visceral stimulation with rest using GLM with the standard hemodynamic response function, we showed that visceral interoception involves BOLD signal changes in the bilateral insula, the anterior and mid-cingulate cortex, the lateral prefrontal cortex, and thalamus. The preliminary brain activation results from these subjects using the proposed MR-compatible, MR-synchronized fluidic visceral stimulation device are also in general agreement with our previous fMRI studies using manual intravesical stimulation [21], [38] and confirms the effectivity of the visceral stimulus.

The proposed device is not only relevant for the study of brain functions in healthy volunteers, but also for the study of functional changes in the brain in neurological visceral pathologies such as the dysfunctions of the lower urinary tract and gastrointestinal tract for which distortions of both top-down modulation of urogenital and gastrointestinal functions, and bottom-up signaling from visceral afferents to the brain have been reported by early investigators (see [39] and also [40] for a comprehensive review). Both the lower urinary and gastrointestinal tract dysfunctions are highly prevalent, causing an enormous economic burden for every health care system and also significantly impair quality of life of the affected patients [41], [42]. Functional neuroimaging studies are an extremely valuable tool to non-invasively investigate such dysfunction in humans. Although the anatomic locations of main brain regions during interoceptive processing have been identified in animal models as well as healthy subjects, the function of the supraspinal regions as an integrated system and its abnormality in the various visceral dysfunctions are less well understood. Potential use of the proposed MR-compatible fluidic visceral stimulation device extends beyond established stimulation protocols and provides increased flexibility for designing new fMRI tasks for different visceral organs that can be stimulated with the fluidic-based methods. For example, the device could be used for stimulating the gastrointestinal tract by the attachment of a naso/orogastric tube similar to the catheter. The alternative approaches to our proposed device are to either have a urologist or gastroenterologist manually perform the organ stimulation during an fMRI experiment or use mental rehearsal or a pharmaceutical drug (e.g., diuretics) to emulate the function of these organs. Performing manual infusion and drainage can be challenging, time-consuming, and prone to human error. Commercially available urodynamic devices that are used during routine filling cystometry in urological departments are neither MR-compatible nor strong enough to provide the required filling speed (e.g., 300-400 mL/min) for fMRI measurements. Other infusion systems that are used in clinical research are notably limited in the programmability of their infusion sequence and none are completely MR-synchronizable. In comparison, our device is specifically built for function inside the MRI environment and its parameters including flow rate and timing are monitored by an MR-compatible sensing unit and can be synchronized with TTL signals from the MRI scanner and adjusted using freely-programmable software based on the experimenters exact requirements.

From an engineering point of view there are two limitations to the current device that can be improved in the next generation of this device. The current configuration of the device can only infuse one type of liquid at a time and lacks the feature for infusing more than one fluid simultaneously or one immediately after another. The current device also lacks a fluid reservoir for refilling during the experiment. Although this device was primarily designed to deliver a maximum fluid volume of 100 mL, larger volumes may be used for visceral stimulation. For example, during intragastric infusion, the dispensed fluid is continuously infused to the stomach over an extended time period and may need to be replenished depending on the stimulation protocol and/or size of the organ. One way to overcome this limit is by using a bigger syringe. The infusion unit of the device can easily accommodate different-size syringes and has an adjustable clamp for securing a syringe of various diameters. However, bigger syringes are usually expensive and not disposable. An alternative is to use a refilling unit or reservoir with the syringe in the infusion unit. Still, a number of issues need to be addressed to ensure the system performance is not compromised with the addition of a reservoir. First, fluid from the reservoir needs to be degassed before injection into the syringe to avoid, e.g., changes in flow rate due to air bubbles. Second, an effective, MR-compatible method needs to be developed for aspiration or refilling of a syringe without requiring concurrent manipulation of a syringe plunger.

In recent years there has been a promising literature on imaging visceral sensations that has not been associated with the traditional neuroimaging studies of interoception (e.g., pain), but can be integrated easily, generating a broader

IEEE Journal of Translational Engineering in Health and Medicine

perspective of neural correlates of interoception. Although we are beginning to understand how the brain processes afferent information from the viscera and internal organs, clearly much research is still required to understand how such interoceptive information is brought to the realm of conscious perception and manifests its influence on our behavior. The use of the automated MR-compatible, MR-synchronized fluidic visceral stimulation devices such as the one we have presented in this paper, can provide increased flexibility for designing and performing visceral stimulation tasks during neuroimaging experiments; hence facilitate our understanding of the brain networks that process interoception.

REFERENCES

[1] A. D. Craig, "Interoception: The sense of the physiological condition of the body," *Current Opinion Neurobiol.*, vol. 13, no. 4, pp. 500–505, 2003.

[2] J. Brooks and I. Tracey, "REVIEW: From nociception to pain perception: Imaging the spinal and supraspinal pathways," *J. Anatomy*, vol. 207, no. 1, pp. 19–33, 2005.

[3] Q. Aziz and D. G. Thompson, "Brain-gut axis in health and disease," *Gastroenterology*, vol. 114, no. 3, pp. 559–578, 1998.

[4] D. Griffiths, S. D. Tadic, W. Schaefer, and N. M. Resnick, "Cerebral control of the bladder in normal and urge-incontinent women," *NeuroImage*, vol. 37, no. 1, pp. 1–7, 2007.

[5] E. A. Mayer, B. D. Naliboff, and A. D. B. Craig, "Neuroimaging of the brain-gut axis: From basic understanding to treatment of functional GI disorders," *Gastroenterology*, vol. 131, no. 6, pp. 1925–1942, 2006.

[6] E. Rickenbacher, M. A. Baez, L. Hale, S. C. Leiser, S. A. Zderic, and R. J. Valentino, "Impact of overactive bladder on the brain: Central sequelae of a visceral pathology," *Proc. Nat. Acad. Sci. USA*, vol. 105, no. 30, pp. 10589–10594, 2008.

[7] O. G. Cameron, "Interoception: The inside story—A model for psychosomatic processes," *Psychosomatic Med.*, vol. 63, no. 5, pp. 697–710, 2001.

[8] D. Vaitl, "Interoception," *Biol. Psychol.*, vol. 42, pp. 1–27, Jan. 1996.

[9] B. Jarrahi, "Neuroimaging of interoception," Ph.D. dissertation, ETH Zurich, Zürich, Switzerland, 2015.

[10] A. D. Craig, "How do you feel? Interoception: The sense of the physiological condition of the body," *Nature Rev. Neurosci.*, vol. 3, pp. 655–666, Aug. 2002.

[11] A. Craig, "Interoception and emotion: A neuroanatomical perspective," in *Handbook of Emotions*, vol. 3, M. Lewis, J. M. Haviland-Jones, and L. F. Barrett, Eds. New York, NY, USA: Guilford Press, 2008, pp. 272–288

[12] B. Jarrahi *et al.*, "Differential functional brain network connectivity during visceral interoception as revealed by independent component analysis of fMRI time-series," *Human Brain Mapping*, vol. 36, pp. 4438–4468, Nov. 2015.

[13] A. R. Damasio, *The Feeling of What Happens: Body and Emotion in the Making of Consciousness*. New York, NY, USA: Orlando, FL, USA: Harcourt Brace Jovanovich, 2000.

[14] B. Jarrahi, D. Mantini, U. Mehnert, and S. Kollias, "Exploring influence of subliminal interoception on whole-brain functional network connectivity dynamics," in *Proc. 37th Annu. Int. Conf. IEEE Eng. Med. Biol. Soc. (EMBC)*, Aug. 2015, pp. 670–674.

[15] B. Jarrahi, D. Mantini, and S. Kollias, "Effect of interoception on intra- and inter-network connectivity of human brain—An independent component analysis of fMRI data," in *Proc. 7th Int. IEEE/EMBS Conf. Neural Eng. (NER)*, Apr. 2015, pp. 320–323.

[16] R. Hölzl, L.-P. Erasmus, and A. Möltner, "Detection, discrimination and sensation of visceral stimuli," *Biol. Psychol.*, vol. 42, pp. 199–214, Jan. 1996.

[17] E. R. Kandel, J. H. Schwartz, and T. M. Jessell, *Principles of Neural Science*, vol. 4. New York, NY, USA: McGraw-Hill, 2000.

[18] D. J. Lassman *et al.*, "Defining the role of cholecystokinin in the lipid-induced human brain activation matrix," *Gastroenterology*, vol. 138, no. 4, pp. 1514–1524, 2010.

[19] L. Van Oudenhove *et al.*, "Fatty acid–induced gut-brain signaling attenuates neural and behavioral effects of sad emotion in humans," *J. Clin. Invest.*, vol. 121, no. 8, pp. 3094–3099, 2011.

[20] M. K. Kern *et al.*, "Identification and characterization of cerebral cortical response to esophageal mucosal acid exposure and distention," *Gastroenterology*, vol. 115, no. 6, pp. 1353–1362, 1998.

[21] U. Mehnert *et al.*, "Brain activation in response to bladder filling and simultaneous stimulation of the dorsal clitoral nerve—An fMRI study in healthy women," *NeuroImage*, vol. 41, no. 3, pp. 682–689, 2008.

[22] R. B. Buxton, E. C. Wong, and L. R. Frank, "Dynamics of blood flow and oxygenation changes during brain activation: The balloon model," *Magn. Reson. Med.*, vol. 39, pp. 855–864, Jun. 1998.

[23] L. A. Zaremba, "FDA guidance for magnetic resonance system safety and patient exposures: Current status and future considerations," in *Magnetic Resonance Procedures: Health Effects and Safety*, F. G. Shellock, Ed. Boca Raton, FL, USA: CRC Press, 2001, pp. 183–196.

[24] N. Yu and R. Riener, "Review on MR-compatible robotic systems," in *Proc. 1st IEEE/RAS-EMBS Int. Conf. Biomed. Robot. Biomechatronics (BioRob)*, Feb. 2006, pp. 661–665.

[25] K. Chinzei, R. Kikinis, and F. A. Jolesz, "MR compatibility of mechatronic devices: Design criteria," in *Proc. Med. Image Comput. Comput.-Assisted Intervent. (MICCAI)*, 1999, pp. 1020–1030.

[26] G. Schaefers and A. Melzer, "Testing methods for MR safety and compatibility of medical devices," *Minimally Invasive Therapy Allied Technol.*, vol. 15, no. 2, pp. 71–75, 2006.

[27] R. Gassert, D. Chapuis, H. Bleuler, and E. Burdet, "Sensors for applications in magnetic resonance environments," *IEEE/ASME Trans. Mechatronics*, vol. 13, no. 3, pp. 335–344, Jun. 2008.

[28] M. J. Firbank, A. Coulthard, R. M. Harrison, and E. D. Williams, "A comparison of two methods for measuring the signal to noise ratio on MR images," *Phys. Med. Biol.*, vol. 44, no. 12, p. N261, 1999.

[29] K. Murphy, J. Bodurka, and P. A. Bandettini, "How long to scan? The relationship between fMRI temporal signal to noise ratio and necessary scan duration," *NeuroImage*, vol. 34, pp. 565–574, Jan. 2007.

[30] T. B. Parrish, D. R. Gitelman, K. S. LaBar, and M.-M. Mesulam, "Impact of signal-to-noise on functional MRI," *Magn. Reson. Med.*, vol. 44, no. 6, pp. 925–932, 2000.

[31] R. R. Price *et al.*, "Quality assurance methods and phantoms for magnetic resonance imaging: Report of AAPM nuclear magnetic resonance Task Group No. 1," *Med. Phys.*, vol. 17, no. 2, pp. 287–295, 1990.

[32] G. Schaefers, "Testing MR safety and compatibility," *IEEE Eng. Med. Biol. Mag.*, vol. 27, no. 3, pp. 23–27, May/Jun. 2008.

[33] R. C. Oldfield, "The assessment and analysis of handedness: The Edinburgh inventory," *Neuropsychologia*, vol. 9, no. 1, pp. 97–113, 1971.

[34] B. Jarrahi and J. Wanek, "Design of an fMRI-compatible optical touch stripe based on frustrated total internal reflection," in *Proc. 36th Annu. Int. Conf. IEEE Eng. Med. Biol. Soc. (EMBC)*, Aug. 2014, pp. 4952–4955.

[35] B. Jarrahi, J. Wanek, U. Mehnert, and S. Kollias, "An fMRI-compatible multi-configurable handheld response system using an intensity-modulated fiber-optic sensor," in *Proc. 35th Annu. Int. Conf. IEEE Eng. Med. Biol. Soc. (EMBC)*, Jul. 2013, pp. 6349–6352.

[36] K. J. Friston, A. P. Holmes, K. J. Worsley, J.-P. Poline, C. D. Frith, and R. S. Frackowiak, "Statistical parametric maps in functional imaging: A general linear approach," *Human Brain Mapping*, vol. 2, no. 4, pp. 189–210, 1994.

[37] P. Colombo, A. Baldassarri, M. Del Corona, L. Mascaro, and S. Strocchi, "Multicenter trial for the set-up of a MRI quality assurance programme," *Magn. Reson. Imag.*, vol. 22, pp. 93–101, Jan. 2004.

[38] U. Mehnert, L. Michels, M.-Z. Zempleni, B. Schurch, and S. Kollias, "The supraspinal neural correlate of bladder cold sensation—An fMRI study," *Human Brain Mapping*, vol. 32, no. 6, pp. 835–845, 2011.

[39] E. A. Mayer, "Gut feelings: The emerging biology of gut–brain communication," *Nature Rev. Neurosci.*, vol. 12, pp. 453–466, Aug. 2011.

[40] C. J. Fowler and D. J. Griffiths, "A decade of functional brain imaging applied to bladder control," *Neurourol. Urodyn.*, vol. 29, no. 1, pp. 49–55, 2010.

[41] D. E. Irwin *et al.*, "Population-based survey of urinary incontinence, overactive bladder, and other lower urinary tract symptoms in five countries: Results of the EPIC study," *Eur. Urol.*, vol. 50, pp. 1306–1315, Dec. 2006.

[42] K. Y. Ho, J. Y. Kang, and A. Seow, "Prevalence of gastrointestinal symptoms in a multiracial Asian population, with particular reference to reflux-type symptoms," *Amer. J. Gastroenterol.*, vol. 93, pp. 1816–1822, Oct. 1998.

BEHNAZ JARRAHI (S'08–M'14) received the B.S.E. (*cum laude*) and M.S.E. degrees in biomedical engineering with a concentration in electrical engineering from the University of Michigan, Ann Arbor, USA. In addition, she holds the B.A. (Hons.) degree in brain science, mathematics, and chemistry. She received the Dr. Sc. degree in electrical engineering and information technology from the Eidgenössische Technische Hochschule (ETH), Switzerland. She is currently a Post-Doctoral Scholar in neuroimaging with the Semel Institute for Neuroscience and Human Behavior at the University of California, Los Angeles, USA, where she is studying human brain neuroplasticity.

ROGER GASSERT (S'02–M'06–SM'13) received the M.Sc. degree in microengineering and the Ph.D. degree in neuroscience robotics from the Ecole Polytechnique Fédérale de Lausanne (EPFL), Lausanne, Switzerland, in 2002 and 2006, respectively. He joined ETH Zurich in 2008, where he is currently an Associate Professor of Rehabilitation Engineering. He has made contributions to the field of neuroscience robotics to investigate sensorimotor control and related dysfunctions, as well as to robot-assisted assessment and therapy. His research interests are in physical human–machine interaction, rehabilitation robotics, assistive technology, and the neural control of movement.

JOHANN WANEK received the Ph.D. degree from University College London, U.K. He is currently a Medical Physicist with Balgrist University Hospital, Zurich, and a Research Assistant with the Institute of Evolutionary Medicine, University of Zurich, Switzerland. His primary research interests include the development of MRI-compatible sensors, nanoscale imaging of ancient cells, and quantum effects in cells.

LARS MICHELS was born in Oberhausen, Germany. He received the M.Sc. degree in biology from the University of Bochum, North Rhine-Westphalia (NRW), Germany, in 2002, and the Ph.D. degree in psychology from the University of Münster, NRW, Germany. He was a Post-Doctoral Fellow with the University of Zurich from 2006 to 2010. Since 2010, he has been a Senior Scientist (Oberassistent) with the Institute of Neuroradiology, University Hospital Zurich, Switzerland.

He uses the state-of-the-art, multimodal brain imaging techniques, including fMRI, EEG, spectroscopy, and ASL-MRI to study human brain development, and neurological disorders, such as Alzheimer's disease, attention deficit disorder, migraine, and stroke.

ULRICH MEHNERT received the M.D. degree form the University of Ulm, Germany, in 2005, where he became a fellow of the European Board of Urology in 2014. He is currently a Consultant Urologist with the Department of Neuro-Urology, Balgrist University Hospital, Zurich, Switzerland, the Deputy Head of the Neuro-Urology Research Group with the Spinal Cord Injury Research Laboratory, University of Zurich, Switzerland, and an Assistant Lecturer with the Medical Faculty, University of Zurich. His main research focus is the structural and functional neuroimaging of supraspinal human lower urinary tract control, neurophysiological assessment of human lower urinary tract sensory function, and diagnosis and treatment of lower urinary tract dysfunctions.

Dr. Mehnert is the Vice Chairman of the Swiss Continence Foundation and a member of the Swiss and German Urological Societies, the European Association of Urology, the International Continence Society, and the Forum Urodynamicum.

SPYROS S. KOLLIAS is the Professor of Radiology with specialization in neuro-radiology with the University of Zurich, Switzerland, and the Chief of the MRI Section with the Institute of Neuroradiology, University Hospital Zurich, Switzerland. He was trained in neuroradiology in the USA from 1990 to 1993, initially for one year with the University of California San Francisco, and subsequently for two years with the Children's Hospital Medical Center, University of Cincinnati, OH, USA. He is a member of several medical associations (ASNR and ISMRM) and Group Leader in the Section of Biomedical Technology and Imaging, Neuroscience Center Zurich.

He has authored more than 200 peer-reviewed publications, reviews, letters, and book chapters. He is a Co-Editor of three books in the field of high resolution medical imaging. He is invited as a Lecturer and Faculty Member in several international scientific conferences in the field of neuroradiology and medical imaging. His main interest is the applications of advanced magnetic resonance imaging technology in the diagnosis of neurologic diseases. His research is funded by competitive third-party funds from the Swiss National Foundation, other medical societies, and the industry.